

Mapping the large-angle deviation from Gaussianity in simulated CMB mapsA. Bernui¹ and M. J. Rebouças²¹*Instituto de Ciências Exatas, Universidade Federal de Itajubá, 37500-903 Itajubá–MG, Brazil*²*Centro Brasileiro de Pesquisas Físicas, Rua Dr. Xavier Sigaud 150, 22290-180 Rio de Janeiro–RJ, Brazil*

(Received 24 September 2011; published 18 January 2012)

The detection of the type and level of primordial non-Gaussianity in the CMB data is essential to probe the physics of the early universe. Since one does not expect that a single statistical estimator can be sensitive to all possible forms of non-Gaussianity which may be present in the data, it is important to employ different statistical indicators to study non-Gaussianity of CMB. In recent works we have proposed two new large-angle non-Gaussianity indicators based on skewness and kurtosis of patches of CMB sky sphere, and used them to find significant deviations from Gaussianity in frequency bands and foreground-reduced CMB maps. Simulated CMB maps with assigned type and amplitude of primordial non-Gaussianity are important tools to determine the strength, sensitivity, and limitations of non-Gaussian estimators. Here we investigate whether and to what extent our non-Gaussian indicators have sensitivity to detect non-Gaussianity of local type, particularly with an amplitude within the 7 yr Wilkinson Microwave Anisotropy Probe (WMAP) bounds. We make a systematic study by employing our statistical tools to generate maps of skewness and kurtosis from several thousands of simulated maps equipped with non-Gaussianity of local type of various amplitudes. We show that our indicators can be used to detect large-angle local-type non-Gaussianity only for relatively large values of the nonlinear parameter $f_{\text{NL}}^{\text{local}}$. Thus, our indicators do not have enough sensitivity to detect deviation from Gaussianity with the nonlinear parameter within the 7 yr WMAP bounds. This result, along with the outcomes of frequency bands and foreground-reduced analyses, suggests that non-Gaussianity captured in the previous works by our indicators is not of primordial origin, although it might have a primordial component. We have also made a comparative study of non-Gaussianity of simulated maps and of the full-sky WMAP 7 yr foreground-reduced internal linear combination (ILC)-7 yr map. An outcome of this analysis is that the level of non-Gaussianity of the ILC-7 yr map is higher than that of the simulated maps for $f_{\text{NL}}^{\text{local}}$ within WMAP bounds. This provides quantitative indications on the suitability of the ILC-7 yr map as Gaussian reconstruction of the full-sky CMB.

DOI: [10.1103/PhysRevD.85.023522](https://doi.org/10.1103/PhysRevD.85.023522)

PACS numbers: 98.80.Es, 98.70.Vc, 98.80.–k

I. INTRODUCTION

The statistical properties of the temperature anisotropies of CMB radiation and of the large-scale structure of the Universe offer a powerful probe of the physics of the early universe [1–4]. Thus, for example, although a convincing detection of a significant level of primordial non-Gaussianity of local type ($f_{\text{NL}}^{\text{local}} \gg 1$) in CMB data would not rule out all inflationary models, it would exclude the entire class of single scalar field models regardless of the form of kinetic term, potential, or initial vacuum state [1,5]. Such a detection, however, would be consistent with some alternative models of the physics of the early universe, and also with other nonstandard inflationary scenarios. On the other hand, a convincing null detection of primordial non-Gaussianity of local type ($f_{\text{NL}}^{\text{local}} \simeq 0$) would rule out the current alternative models of the primordial universe (see, e.g., Refs. [1–3,6]). Thus, a detection or null detection of primordial non-Gaussianity of local type in the CMB data is crucial not only to discriminate or even exclude classes of inflationary models, but also to test alternative scenarios, offering therefore an important window into the physics of the early universe.

However, there are various effects that can produce non-Gaussianity. Among them, the most significant are possibly unsubtracted diffuse foreground emission [7,8], unresolved point sources [9], possible systematic errors [10], and secondary anisotropies such as gravitational weak lensing and the Sunyaev-Zeldovich effect (see, e.g., Refs. [1,2]).¹ In this way, the accurate extraction of a possible primordial non-Gaussianity is a challenging observational and statistical enterprise.

In the search for non-Gaussianity in CMB data, different statistical tools can, in principle, provide information about distinct forms of non-Gaussianity. On the other hand, one does not expect that a single statistical estimator can be sensitive to all possible forms of non-Gaussianity that may

¹For most of these effects there seems to be no evidence of significant non-Gaussian contamination within Wilkinson Microwave Anisotropy Probe (WMAP) sensitivity. Nevertheless, this is not guaranteed to hold true for the PLANCK experiment [11], due to its much higher sensitivity [2]. Cosmic variance further complicates the problem, since some non-Gaussianity may arise from the uniqueness of the observed CMB sky. Deviation from Gaussianity may also have a cosmic topology origin [12].

be present in CMB data. It is therefore important to test CMB data for deviations from Gaussianity by using different statistical tools in order to quantify or constrain the amount of any non-Gaussian signals in the data, and extract information on their possible origins. This has motivated a great deal of effort that has recently gone into the search for non-Gaussianity in CMB maps by employing several statistical estimators (an incomplete list of references is given in the recent reviews [1–3], and also in Refs. [13–15]).

In recent papers [13,14] we have proposed two new large-angle non-Gaussianity estimators, which are based upon the skewness and kurtosis of the patches (spherical caps) of the CMB sky sphere. By scanning the CMB sphere with evenly distributed spherical caps, and calculating the skewness S and kurtosis K for each cap, one can have measures of the departure from Gaussianity on large angular scales. Using this procedure we have carried out analyses of large-angle deviation from Gaussianity in both band and foreground-reduced maps with and without the KQ75 mask recommended by the Wilkinson Microwave Anisotropy Probe (WMAP) team for Gaussianity studies of CMB data [13,14]. Thus, we have found, for example, significant departure from Gaussianity in all full-sky band maps, while for the Q, V, W maps with the KQ75 mask, the CMB data are consistent with Gaussianity. The K and Ka maps, however, show an important deviation from Gaussianity even with a KQ75 mask. For the full-sky foreground-reduced maps [16–19] we have found a significant deviation from Gaussianity, which varies with the cleaning process, as measured by our indicators [14].

Simulated CMB maps equipped with assigned primordial non-Gaussianity are essential tools to test the sensitivity and effectiveness of non-Gaussian indicators. They can also be used to study, e.g., the effects of foregrounds and other non-Gaussian contaminants, and also to disclose potential systematics. In a recent paper a new algorithm for generating non-Gaussian CMB temperature maps with non-Gaussianity of the local type has been devised [20]. In the simulated maps the level of non-Gaussianity is adjusted by the dimensionless parameter $f_{\text{NL}}^{\text{local}}$. A set of 1000 CMB temperature simulated maps with the resolution of PLANCK mission [11] for open (unfixed) values of $f_{\text{NL}}^{\text{local}}$ was made available [20].

A pertinent question that arises is whether the indicators proposed in Ref. [13], and used in Refs. [13,14] to detect non-Gaussianity in CMB data, have sufficient sensitivity to detect deviation from non-Gaussianity of local type with an amplitude $f_{\text{NL}}^{\text{local}}$ within the bounds determined by the WMAP team in their latest data release [21]. Our primary aim in this paper is to address this question by extending the results and by complementing the analyses of Refs. [13,14] in three different ways. First, instead of using CMB data, we use our statistical indicators to carry out an analysis of Gaussianity of *simulated* maps equipped with non-

Gaussianity of local type. Second, by using simulated maps with different amplitudes $f_{\text{NL}}^{\text{local}}$, we make a quantitative analysis of the degree of sensitivity of our skewness and kurtosis indicators to detect primordial non-Gaussianity of local type. Third, we make a comparative study of the degrees of non-Gaussianity of simulated maps with different $f_{\text{NL}}^{\text{local}}$'s and the full-sky foreground-reduced 7 yr WMAP internal linear combination (ILC-7 yr) map [16]. An interesting outcome of this comparative analysis is that the level of non-Gaussianity of the ILC-7 yr is considerably higher than that of the simulated maps for $f_{\text{NL}}^{\text{local}}$ within observational bounds [21]. This renders information about the suitability of the ILC-7 yr foreground-reduced map as a Gaussian reconstruction of the CMB full sky.

II. NON-GAUSSIANITY AND SIMULATED MAPS

A. Primordial non-Gaussianity of local type

The first important ingredient in the study of non-Gaussianity is the primordial gravitational curvature perturbations $\zeta(\mathbf{x}, t)$, which were seeded by quantum fluctuations in the very early universe. In the linear order, the primordial curvature perturbation is related to Bardeen's curvature perturbation $\Phi(\mathbf{x}, t)$ [22] in the matter dominated era by $\zeta = (5/3)\Phi$ [23]. The relation with CMB observations is given in the Sachs-Wolfe limit, where $\Delta T/T = -\Phi/3 = -\zeta/5$ holds [24].

The lower order statistics able to distinguish non-Gaussian from Gaussian distributions is the three-point correlation function. Primordial non-Gaussianity can then be described in terms of the three-point correlation function of the curvature perturbations $\Phi(\mathbf{x})$ or of its Fourier transform $\Phi(\mathbf{k})$ by using the ensemble average. Thus, the three-point correlation function counterpart in Fourier space—the so-called bispectrum—takes the form

$$\langle \Phi(\mathbf{k}_1)\Phi(\mathbf{k}_2)\Phi(\mathbf{k}_3) \rangle = \delta^3(\mathbf{k}_{123})B_\Phi(k_1, k_2, k_3), \quad (1)$$

where $\delta^{(3)}(\mathbf{k}_{123}) \equiv \delta^{(3)}(\mathbf{k}_1 + \mathbf{k}_2 + \mathbf{k}_3)$ enforces that the wave vectors in Fourier space have to close to form a triangle, i.e., $\mathbf{k}_1 + \mathbf{k}_2 + \mathbf{k}_3 = 0$. Thus, the bispectrum is a function of the triplet defined by the magnitude of the wave numbers (k_1, k_2, k_3) .

In the examination of primordial non-Gaussianity, the bispectrum of curvature is rewritten in the form

$$\begin{aligned} B_\Phi(\mathbf{k}_1, \mathbf{k}_2, \mathbf{k}_3) &= \langle \Phi(\mathbf{k}_1)\Phi(\mathbf{k}_2)\Phi(\mathbf{k}_3) \rangle \\ &= f_{\text{NL}}(2\pi)^3 \delta^3(\mathbf{k}_{123})F(k_1, k_2, k_3), \end{aligned} \quad (2)$$

where f_{NL} is an overall amplitude (dimensionless) parameter,² which can be constrained by the CMB data, and where $F(k_1, k_2, k_3)$ is the so-called shape of the bispectrum and

²The subscript ‘‘NL’’ stands for nonlinear. This notation arises because an often-used phenomenological parametrization for the non-Gaussianity of $\Phi(\mathbf{x})$ can be written as a nonlinear transformation of a Gaussian field (see below for more details).

encodes the functional dependence of the bispectrum on the triangular configurations. The bispectrum shape is used to specify the configuration of the wave vectors of curvature perturbations that give the highest contributions to the amplitude of the bispectrum. In this way, the bispectra are usually classified according to shapes of the triangles that give rise to the highest non-Gaussian signal. The most studied shapes are (i) local, where the bispectrum is maximum on the squeeze triangle configuration, $k_1 \approx k_2 \gg k_3$; (ii) equilateral, with the bispectrum maximized on the equilateral limit $k_1 \approx k_2 \approx k_3$; and (iii) orthogonal, where the bispectrum has a positive peak at the equilateral configuration and a negative valley along the flattened (elongated) triangular configuration, $k_3 \approx k_1 + k_2$ [1]. Predictions for both the amplitude f_{NL} and the shape of $B_\Phi(k_1, k_2, k_3)$ depend on the early universe models, which makes apparent the power of the bispectrum as a tool to probe models of the primordial universe.

In this paper we shall deal with non-Gaussianity of local type, which is the most studied type of deviation from Gaussianity. For this type of primordial non-Gaussianity the curvature perturbation in the real space can be split into two components: the linear term Φ_L (representing the Gaussian component) plus a non-Gaussian second term, namely,³

$$\Phi(\mathbf{x}) = \Phi_L(\mathbf{x}) + f_{\text{NL}}^{\text{local}}(\Phi_L^2(\mathbf{x}) - \langle \Phi_L^2(\mathbf{x}) \rangle), \quad (3)$$

where both sides are evaluated at the same spatial location \mathbf{x} .

Finally, we recall that the latest WMAP constraints reported on $f_{\text{NL}}^{\text{local}}$ at the 95% confidence level are given by $-10 < f_{\text{NL}}^{\text{local}} < 74$ [21]. These bounds will be used in our analyses in one of the following sections.

B. Simulated CMB maps

The first simulated CMB temperature maps endowed with primordial non-Gaussianity introduced through a non-Gaussian parameter f_{NL} were generated by the WMAP team and reported in Ref. [9]. The WMAP algorithm was generalized so as to improve computational speed and accuracy, and also to include polarization maps in Ref. [26] (see also Ref. [27]). More recently, Elsner and Wandelt [20] presented a new algorithm and generated 1000 high-angular resolution simulated non-Gaussian CMB temperature and polarization maps with non-Gaussianities of the local type, for which the level of non-Gaussianity is determined by the parameter $f_{\text{NL}}^{\text{local}}$. In their algorithm a simulated map with a desired level of non-Gaussianity $f_{\text{NL}}^{\text{local}}$ is such that the spherical harmonic coefficients are given by

$$a_{\ell m} = a_{\ell m}^L + f_{\text{NL}}^{\text{local}} \cdot a_{\ell m}^{\text{NL}}, \quad (4)$$

where $a_{\ell m}^L$ and $a_{\ell m}^{\text{NL}}$ are, respectively, the linear and nonlinear spherical harmonic coefficients of the simulated CMB temperature maps.

In the next sections we shall use the set of 6000 CMB temperature simulated linear and nonlinear component maps, generated for an arbitrary (unfixed) value of $f_{\text{NL}}^{\text{local}}$, which was made available in Ref. [20]⁴ with the resolution of the PLANCK mission [11].

III. NON-GAUSSIANITY INDICATORS AND ASSOCIATED MAPS

To make our paper clear and self-contained, in this section we describe the two statistical non-Gaussianity indicators and their associated maps, which can be calculated from either simulated or real CMB temperature (input) maps. The procedure delineated here will be used in the following sections to investigate large-angle deviation from Gaussianity.

The most important underlying idea in the construction of our non-Gaussianity indicators and the associated maps is that one can access the deviation from Gaussianity of the CMB temperature fluctuations by calculating the skewness S and the kurtosis K , which measure, respectively, the symmetry about the mean temperature and the non-Gaussian degree of peakness of the temperature distribution.

Clearly the calculation of S and K from the whole CMB sky sphere of temperature fluctuations data would be a crude approach to measure the complexity of the non-Gaussianity of the CMB map. However, instead of having just two dimensionless numbers, one can go further by taking a discrete set of points $j = 1, \dots, N_c$ homogeneously distributed on the CMB sky sphere S^2 as the center of spherical caps of aperture γ (say), and calculate S_j and K_j for each cap j of the CMB temperature sky sphere. The values S_j and K_j can then be taken as measures of the non-Gaussianity in the direction (θ_j, ϕ_j) of the center of the spherical cap j . Such calculations for the individual caps thus provide quantitative information ($2N_c$ values) about non-Gaussianity of the CMB data.

The above procedure is a constructive way of defining on S^2 two discrete functions $S(\theta, \phi)$ and $K(\theta, \phi)$ that measure departure from Gaussianity of a CMB temperature (input) map. In other words, these functions can be constructed from an input CMB map through the following steps [13]:

- (i) Take a discrete finite set of points $j = 1, \dots, N_c$ homogeneously distributed on the sky sphere of a CMB input map as the centers of spherical caps of a chosen aperture γ , and calculate for each cap j the skewness and kurtosis given, respectively, by

³It should be noted, however, that this is not the only way to produce the bispectrum of local type. A multifield curvaton inflation, for example, can also produce a bispectrum of local type [25].

⁴<http://planck.mpa-garching.mpg.de/cmb/fnl-simulations>.

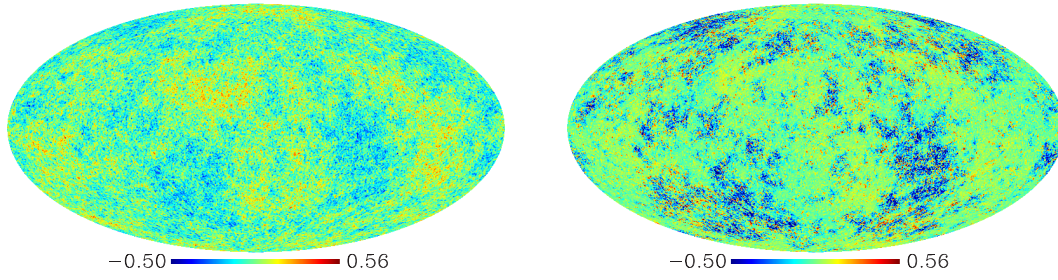


FIG. 1 (color online). The left panel shows a simulated Gaussian CMB map ($f_{\text{NL}}^{\text{local}} = 0$), while the right panel depicts a non-Gaussian simulated CMB map calculated for $f_{\text{NL}}^{\text{local}} = 5000$. Temperatures are in mK .

$$S_j = \frac{1}{N_p \sigma_j^3} \sum_{i=1}^{N_p} (T_i - \bar{T})^3, \quad (5)$$

$$K_j = \frac{1}{N_p \sigma_j^4} \sum_{i=1}^{N_p} (T_i - \bar{T})^4 - 3, \quad (6)$$

where T_i is the temperature at the i th pixel, \bar{T}_j is the CMB mean temperature of the j th spherical cap, N_p is the number of pixels in the cap j , and $\sigma^2 = (1/N_p) \sum_{i=1}^{N_p} (T_i - \bar{T})^2$ is the standard deviation. Clearly, the whole set of values S_j and K_j (for all j) obtained through this discrete *scanning* calculation process, along with the angular coordinate of the center of the caps (θ_j, ϕ_j), can be taken as measures of non-Gaussianity in the directions of the center of spherical caps j .

- (ii) Patching together the S_j and K_j values for all spherical caps j , one has two discrete functions $S = S(\theta, \phi)$ and $K = K(\theta, \phi)$ defined over a two-sphere S^2 . These functions provide measurements of the non-Gaussianity as a function of (θ, ϕ) . The Mollweide projections of the functions $S = S(\theta, \phi)$ and $K = K(\theta, \phi)$ are nothing but skewness and kurtosis maps (hereafter denoted by S map and K map).

Clearly, the functions $S = S(\theta, \phi)$ and $K = K(\theta, \phi)$ can be expanded into their spherical harmonics. Thus, for example, for $S = S(\theta, \phi)$ one has

$$S(\theta, \phi) = \sum_{\ell=0}^{\infty} \sum_{m=-\ell}^{\ell} b_{\ell m} Y_{\ell m}(\theta, \phi), \quad (7)$$

and the corresponding angular power spectrum

$$S_{\ell} = \frac{1}{2\ell + 1} \sum_m |b_{\ell m}|^2, \quad (8)$$

which can be used to quantify the amplitude (level) and angular scale of the deviation from Gaussianity. In this paper we shall use the power spectra S_{ℓ} and K_{ℓ} to estimate the departure from Gaussianity and calculate the statistical significance of such a deviation by comparison with the

corresponding power spectra calculated from S and K maps obtained from input Gaussian maps ($f_{\text{NL}}^{\text{local}} = 0$).

In the next section we will use these statistical indicators to carry out analyses of Gaussianity of *simulated* maps endowed with non-Gaussianity of local type of different levels to test the sensitivity of S and K indicators to detect primordial non-Gaussianity of local type. Furthermore, we will make a comparative study of the degrees of non-Gaussianity of different simulated maps and the ILC-7 yr WMAP map.

IV. NON-GAUSSIANITY AND SENSITIVITY OF S AND K INDICATORS

A. Analyses and results for simulated maps

It is clear from the previous section that in order to study the sensitivity of the non-Gaussianity indicators S and K , that is, to construct the functions $S = S(\theta, \phi)$ and $K = K(\theta, \phi)$ and the associated S and K maps, we need CMB input maps. The input maps used in our analyses in this section are high-angular resolution-simulated CMB temperature maps endowed with non-Gaussianities of the local type introduced through different values of the dimensionless amplitude parameter $f_{\text{NL}}^{\text{local}}$.

Figure 1 shows two examples of such simulated CMB maps. The left panel gives a Gaussian map $f_{\text{NL}}^{\text{local}} = 0$, while the right panel shows a non-Gaussian map for $f_{\text{NL}}^{\text{local}} = 5000$. We have taken these values for $f_{\text{NL}}^{\text{local}}$ as an illustrative example that makes the non-Gaussian effects visible to the naked eye through the comparison of these simulated maps.

Figure 2 gives an illustration of typical skewness S (left panel) and kurtosis K (right panel) maps, generated from input CMB simulated maps for $f_{\text{NL}}^{\text{local}} = 500$ (first row) and $f_{\text{NL}}^{\text{local}} = 0$ (second row). The non-Gaussian maps show spots with higher and lower values of $S(\theta, \phi)$ and $K(\theta, \phi)$, which suggest *large-angle* dominant multipole components (low ℓ) in these maps.⁵ In our calculations

⁵We have also calculated similar maps from the simulated maps for the other values of $f_{\text{NL}}^{\text{local}}$. These maps, however, provide only qualitative information, and to avoid repetition we only depict maps of Fig. 2 for illustrative purposes.

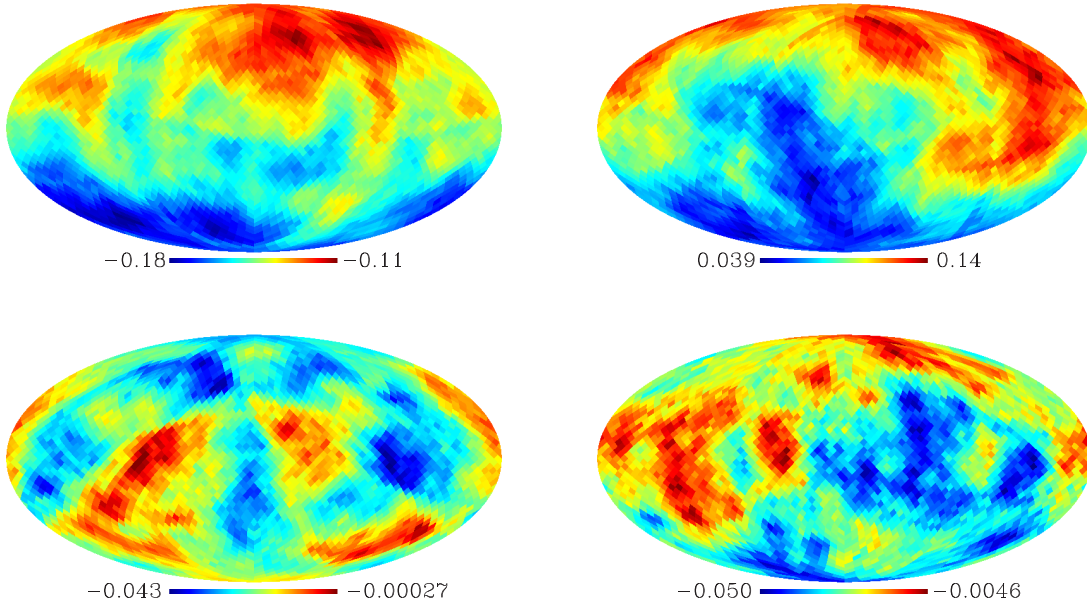


FIG. 2 (color online). Examples of skewness (left panels) and kurtosis (right panels) indicator maps calculated from simulated maps with, respectively, $f_{\text{NL}}^{\text{local}} = 500$ (first row) and $f_{\text{NL}}^{\text{local}} = 0$ (second row).

of all S maps and K maps, to minimize the statistical noise, we have scanned the CMB sphere with $N_c = 3072$ spherical caps of aperture $\gamma = 90^\circ$, centered at points homogeneously distributed on the two-sphere.

To obtain *quantitative* large-angle-scale information, as a first test of the sensitivity of S and K indicators, for each of the following values of the nonlinear parameter— $f_{\text{NL}}^{\text{local}} = 0, 500, 1000, 5000$ —we have generated 1000 simulated CMB maps, totalizing 4000 simulated maps. From each set of 1000 simulated input CMB maps (fixed $f_{\text{NL}}^{\text{local}}$ for each set) we have calculated 1000 S maps and 1000 K maps, from which we computed the associated power spectra, namely, S_ℓ^i and K_ℓ^i , where $i = 1, \dots, 1000$ is an enumeration index, and $\ell = 1, \dots, 10$ is the range of multipoles we have focused on in this paper.⁶ The low ℓ multipole mean components S_ℓ and K_ℓ are then obtained by averaging over 1000 power spectra calculated from simulated maps with the different values of $f_{\text{NL}}^{\text{local}}$. The statistical significance of these power spectra is estimated by comparing the values of S_ℓ and K_ℓ obtained from input maps generated for $f_{\text{NL}}^{\text{local}} = 500, 1000, 5000$ with the values of the corresponding power spectra S_ℓ and K_ℓ obtained from the Gaussian simulated map ($f_{\text{NL}}^{\text{local}} = 0$).

Let us describe with some details the calculations of an average power spectrum. For the sake of brevity, we focus on the skewness indicator S along with a set of 1000 simulated non-Gaussian input maps computed for a non-

linear parameter $f_{\text{NL}}^{\text{local}} = 500$, for example.⁷ Following the two step procedure described in Sec. III, from these 1000 simulated CMB maps we calculated 1000 S maps, from which we computed 1000 power spectra S_ℓ^i in order to have the average values $S_\ell = (1/1000) \sum_{i=1}^{1000} S_\ell^i$. From this MC process we have at the end ten mean multipole values S_ℓ ($\ell = 1, \dots, 10$), each of which is then used for a comparison with the corresponding average multipole value S_ℓ calculated by a similar procedure from Gaussian simulated maps ($f_{\text{NL}}^{\text{local}} = 0$). This allows the evaluation of the statistical significance of S_ℓ by quantifying the goodness of fit for S_ℓ with $f_{\text{NL}}^{\text{local}} \neq 0$ and S_ℓ calculated for $f_{\text{NL}}^{\text{local}} = 0$ (Gaussian maps).

Figure 3 shows the average power spectra of the skewness S_ℓ (left panel) and kurtosis K_ℓ (right panel), for $\ell = 1, \dots, 10$, calculated from simulated Gaussian ($f_{\text{NL}}^{\text{local}} = 0$) maps, and from CMB maps equipped with non-Gaussianity of the local type for which $f_{\text{NL}}^{\text{local}} = 500, 1000, 5000$. The 95% confidence level, obtained from the S and K maps calculated from the Gaussian CMB simulated maps, is indicated in this figure by the dotted line.

To the extent that the average S_ℓ and K_ℓ obtained from input simulated CMB maps endowed with $f_{\text{NL}}^{\text{local}} = 500$ are within 95% Monte Carlo (MC) average values of S_ℓ and K_ℓ for $f_{\text{NL}}^{\text{local}} = 0$, Fig. 3 shows that our indicators are not suitable to detect primordial non-Gaussianity of local type in CMB maps smaller than this level. However, this figure also shows that they can be effectively employed to detect higher levels of non-Gaussianity of local type. These

⁶The values of ℓ_{max} for S_ℓ and K_ℓ depend on the resolution of S and K maps, which clearly depend upon the number of spherical caps used in the scanning process. For $N_c = 3072$ one can go up to $\ell_{\text{max}} = 45$.

⁷A completely similar procedure can clearly be used for the kurtosis indicator K along with other values of $f_{\text{NL}}^{\text{local}}$.

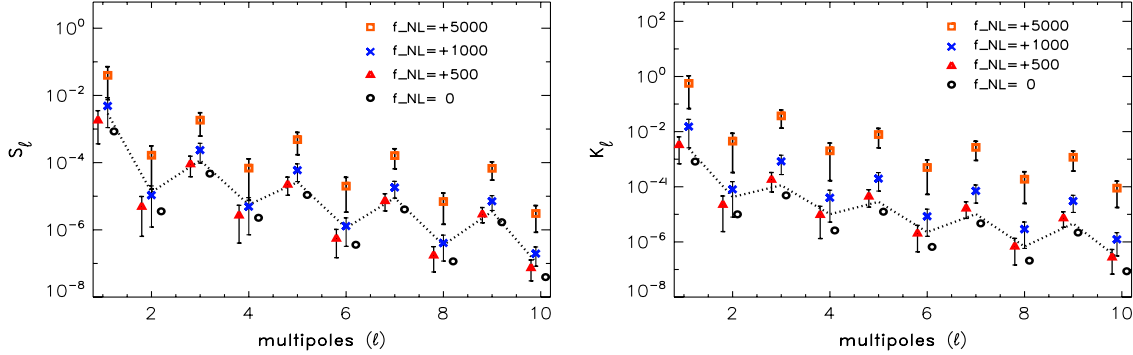


FIG. 3 (color online). Low ℓ average power spectra of skewness S_ℓ (left panel) and kurtosis (right panel) K_ℓ calculated from the Gaussian ($f_{\text{NL}}^{\text{local}} = 0$) and non-Gaussian ($f_{\text{NL}}^{\text{local}} = 500, 1000,$ and 5000) input simulated CMB maps. The 1σ error bars are also indicated with a small horizontal shift to avoid overlap. The 95% confidence level relative to the Gaussian maps is indicated by the dotted line.

results square with the statistical analysis we shall report in the remainder of this paper, particularly with the χ^2 test of goodness of fit.

To have an overall assessment power spectra S_ℓ and K_ℓ , calculated from the input simulated non-Gaussian maps equipped with primordial non-Gaussianity with nonlinear parameter $f_{\text{NL}}^{\text{local}} = 500, 1000, 5000$, we have made a χ^2 test to find out the goodness of fit for S_ℓ and K_ℓ multipole values as compared to the MC mean multipole values obtained from S and K maps of the Gaussian ($f_{\text{NL}}^{\text{local}} = 0$) simulated maps. In each case, this gives a number that quantifies collectively the deviation from Gaussianity. For the power spectra S_ℓ and K_ℓ we found the values given in Table I for the ratio (reduced χ^2) χ^2/dof (dof stands for degrees of freedom) for the power spectra calculated from non-Gaussianity of local type with $f_{\text{NL}}^{\text{local}} = 500, 1000, 5000$. Moreover, the greater the reduced χ^2 values (hereafter denoted simply by χ^2), the smaller the χ^2 probabilities, that is, the probability that the multipole values S_ℓ and K_ℓ and the mean multipole values obtained from the Gaussian maps ($f_{\text{NL}}^{\text{local}} = 0$) agree.

Thus, Table I, along with Fig. 3, shows that the statistical indicators S and K can clearly detect deviation from Gaussianity of simulated maps endowed with primordial non-Gaussianity of local type with $f_{\text{NL}}^{\text{local}} \gtrsim 500$.

TABLE I. Results of the reduced χ^2 test of the goodness of fit for S_ℓ and K_ℓ calculated from the maps with different levels of non-Gaussianity as compared with the corresponding mean values obtained from MC simulated CMB input maps with $f_{\text{NL}}^{\text{local}} = 0$.

Non-Gaussian parameter	χ^2 for S_ℓ	χ^2 for K_ℓ
$f_{\text{NL}}^{\text{local}} = 500$	2.10	2.12×10
$f_{\text{NL}}^{\text{local}} = 1000$	3.02×10	5.50×10^2
$f_{\text{NL}}^{\text{local}} = 5000$	5.54×10^3	1.31×10^6

A question that arises at this point is whether S and K indicators have sufficient sensitivity to detect deviation from non-Gaussianity for the values of the non-Gaussian parameter within the WMAP 7 yr bounds $-10 < f_{\text{NL}}^{\text{local}} < 74$ [21]. Table II makes clear that for maps with $f_{\text{NL}}^{\text{local}}$ within this interval, one has a negligible value of χ^2 , which makes it apparent that there is no significant overall departure of power spectra S_ℓ and K_ℓ for $f_{\text{NL}}^{\text{local}} = -10$ and $f_{\text{NL}}^{\text{local}} = 74$ from the corresponding MC mean power spectra obtained from the Gaussian ($f_{\text{NL}}^{\text{local}} = 0$) maps, in agreement with the nearly overlapping symbols of Fig. 4. This makes it apparent that the bispectrum based estimator that was employed by the WMAP team [9,21] is more sensitive to primordial non-Gaussianity of local type than the S and K indicators employed in the present paper (see also the related references [28]). Thus, for example, the deviation from Gaussianity as captured by our indicators S and K for simulated maps with $f_{\text{NL}}^{\text{local}} = 74$ is 4 orders of magnitude smaller than that for maps with $f_{\text{NL}}^{\text{local}} = 1000$.

To close this section, some words of clarification regarding the forthcoming CMB data from the PLANCK mission are in order. PLANCK combines high-angular resolution and sensitivity with a wide frequency coverage (20 GHz to 1000 GHz) and will allow greatly improved foreground removal, thereby reducing many sources of non-Gaussian contaminants. The latest constraint on $f_{\text{NL}}^{\text{local}}$ from the

TABLE II. Results of the χ^2 test of the goodness of fit for S_ℓ and K_ℓ calculated from the maps with $f_{\text{NL}}^{\text{local}} = -10$ and $f_{\text{NL}}^{\text{local}} = 74$ relative to the corresponding mean values obtained from MC simulated CMB input maps with $f_{\text{NL}}^{\text{local}} = 0$.

Non-Gaussian parameter	χ^2 for S_ℓ	χ^2 for K_ℓ
$f_{\text{NL}}^{\text{local}} = -10$	2.80×10^{-5}	4.80×10^{-5}
$f_{\text{NL}}^{\text{local}} = +74$	1.10×10^{-3}	1.00×10^{-2}

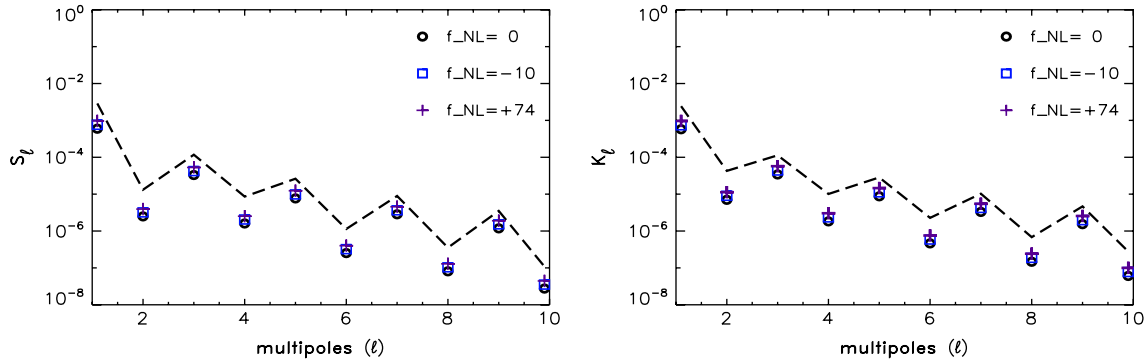


FIG. 4 (color online). Low ℓ average power spectra of skewness S_ℓ (left panel) and kurtosis (right panel) K_ℓ calculated from the Gaussian ($f_{\text{NL}}^{\text{local}} = 0$) and non-Gaussian simulated CMB maps for $f_{\text{NL}}^{\text{local}} = -10$ and $f_{\text{NL}}^{\text{local}} = 74$. The 95% confidence level relative to the Gaussian maps is indicated by the dashed line.

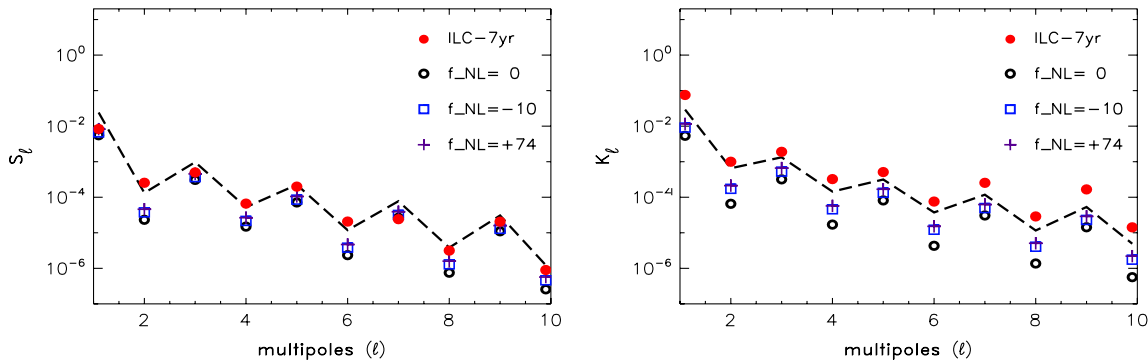


FIG. 5 (color online). Low ℓ mean power spectra of skewness S_ℓ (left panel) and kurtosis (right panel) K_ℓ calculated from ILC-7 yr Gaussian ($f_{\text{NL}}^{\text{local}} = 0$) and non-Gaussian simulated CMB maps for $f_{\text{NL}}^{\text{local}} = -10$ and $f_{\text{NL}}^{\text{local}} = 74$. In these calculations we have used simulated maps with the same smoothed 1° resolution of the ILC-7 yr WMAP map. The 95% confidence level relative to the Gaussian maps is indicated by the dashed line.

WMAP-7 yr is $f_{\text{NL}}^{\text{local}} = 32 \pm 21$ (68% confidence level), and from PLANCK we expect $\Delta f_{\text{NL}}^{\text{local}} \simeq 5$. This includes cosmic variance and the detector noise [29]. For a similar reduction at 2σ confidence level, for example, the non-Gaussian procedure of our paper does not have enough sensibility to detect deviation from Gaussianity within the resulting PLANCK range of $f_{\text{NL}}^{\text{local}}$. A preliminary analysis shows that a new procedure with a different way of scanning input maps (through large pixels cells) seems to be capable of detecting such a tiny deviation from Gaussianity, i.e. within the narrow range of $f_{\text{NL}}^{\text{local}}$ expected from the PLANCK mission.

B. Analyses and results for simulated and data maps

Besides the five frequency band 7 yr maps released—K (22.8 GHz), Ka (33.0 GHz), Q (40.7 GHz), V (60.8 GHz), and W (93.5 GHz)—the WMAP has also produced a full-sky foreground-reduced ILC-7 yr map, which is formed

from a weighted linear combination of these five frequency band maps in which the weights are chosen in order to minimize the galactic foreground contribution.

The first-year ILC map has been explicitly stated as inappropriate for CMB scientific studies [30], but in the subsequent ILC versions, including the ILC-7 yr, a bias correction has been incorporated as part of the foreground cleaning process, and the WMAP team suggested that these maps are suitable for use in large angular scale (low ℓ) analyses, although they have not performed non-Gaussian tests on these versions of the ILC maps [16,19,31].

In a recent paper [14] we have performed an analysis of Gaussianity of all the available full-sky foreground-reduced maps by using S and K non-Gaussianity indicators in the search for departure from Gaussianity on large angular scales [13]. We have shown that the full-sky foreground-reduced WMAP maps, including the ILC-7 yr maps [16], present a significant deviation from

TABLE III. Results of the reduced χ^2 test of the goodness of fit for S_ℓ and K_ℓ calculated from ILC-7 yr and MC simulated maps for the 7 yr WMAP lower and upper bound values of $f_{\text{NL}}^{\text{local}}$. In these calculations we have used simulated maps with the same smoothed 1° resolution of the ILC-7 yr WMAP map. These values quantify collectively the deviation from Gaussianity relative to MC Gaussian simulated maps ($f_{\text{NL}}^{\text{local}} = 0$).

Map	χ^2 for S_ℓ	χ^2 for K_ℓ
$f_{\text{NL}}^{\text{local}} = -10$	6.80×10^{-2}	3.80×10^{-1}
$f_{\text{NL}}^{\text{local}} = +74$	7.10×10^{-2}	4.24×10^{-1}
ILC	8.96	5.88×10

Gaussianity, in agreement with the results of Ref. [13,14,32].

An interesting question that arises here is how one compares the level of deviation from Gaussianity of the ILC maps with the level of primordial non-Gaussianity of local type with different amplitude parameters $f_{\text{NL}}^{\text{local}}$.⁸ We undertake this question by using our indicators to carry out a comparative analysis of non-Gaussianity of simulated maps for the values of non-Gaussian parameters equal to the bounds reported by the WMAP team, and the ILC-7 yr map.

Figure 5 shows the low ℓ mean power spectra of the skewness S_ℓ (left panel) and kurtosis K_ℓ (right panel), calculated from simulated Gaussian ($f_{\text{NL}}^{\text{local}} = 0$) and non-Gaussian maps for $f_{\text{NL}}^{\text{local}} = -10, 74$, which are the lower and upper bounds of the nonlinear parameter reported recently by WMAP [21]. We have calculated the power spectra by using 1000 maps for each value of $f_{\text{NL}}^{\text{local}}$. This figure also displays S_ℓ and K_ℓ computed from the full-sky foreground-reduced ILC-7 yr map. Figure 5 gives a clear indication that the deviation from Gaussianity of the ILC-7 yr map (detected by S and K) is greater than the non-Gaussianity of MC simulated maps for the lower and upper bounds of $f_{\text{NL}}^{\text{local}}$ provided by WMAP [21]. Clearly, in the calculation of the mean power spectra S_ℓ K_ℓ of Fig. 5, we have used simulated maps with the same smoothed 1° resolution of the ILC-7 yr WMAP map.

In order to compare quantitatively the deviation from Gaussianity, we have calculated the χ^2 test of the goodness of fit for S_ℓ and K_ℓ calculated from ILC-7 yr along with the simulated maps for $f_{\text{NL}}^{\text{local}} = -10, 74$ relative to the mean power spectra of Gaussian maps. We have gathered together in Table III the obtained values for the reduced χ^2 . Figure 5, along with Table III, shows, on the one hand, a

⁸We note that as the simulated CMB maps are full-sky maps, and sky cuts induce bias in the Gaussianity analyses, in order to make a comparative analysis of Gaussianity between simulated and data maps, a simple suitable choice of CMB data map is to take the equally full-sky data maps such as the ILC-7 yr. Nevertheless, in the Appendix we present a comparative analysis between maps with $f_{\text{NL}}^{\text{local}}$ for the WMAP-7 yr bounds and the Q , V , and W frequency maps.

significant deviation from Gaussianity in the 7 yr full-sky foreground-reduced ILC-7 yr map, in agreement with the statistical analysis made in Ref. [14]. On the other hand, it is apparent that the level of non-Gaussianity of the ILC-7 yr maps is higher than that of the simulated non-Gaussian maps with $f_{\text{NL}}^{\text{local}}$ equal to the bounds of the WMAP-7 yr data. This comparison provides indications of the suitability of the foreground-reduced ILC-7 yr map as a Gaussian reconstruction of the CMB sky.

V. CONCLUDING REMARKS

The physics of the early universe can be probed by measurements of statistical properties of primordial fluctuations, which are the seeds for the temperature CMB anisotropies. Thus, the study of non-Gaussianity of these anisotropies offers a powerful approach to probe the physics of the primordial universe. It is essential, for example, to discriminate or even exclude classes of inflationary models, and also to test alternative scenarios of the primordial universe.

Since one does not expect a single statistical estimator to be sensitive to all possible forms of non-Gaussianity, it seems important to test CMB data for deviations from Gaussianity by employing different statistical tools to quantify or constrain the amount of any non-Gaussian signals in the data, and extract information concerning their potential origins.

In recent papers [13,14] we proposed two new large-angle non-Gaussianity indicators, based on skewness and kurtosis of large-angle patches of the CMB sky sphere and used them to find significant large-angle deviations from Gaussianity in masked frequency bands and foreground-reduced CMB maps.

Simulated CMB maps with an assigned primordial non-Gaussianity of a given type and amplitude are important tools to study the sensitivity, power, and limitations of non-Gaussian estimators. They can also be used to calibrate non-Gaussian statistical indicators, and to study the effects of foregrounds and other non-Gaussian contaminants.

In this paper we have addressed the question as to whether the non-Gaussian indicators proposed in Refs. [13,14] have sufficient sensitivity to detect non-Gaussianity of local type, particularly with amplitude $f_{\text{NL}}^{\text{local}}$ within the 7 yr WMAP bounds [21]. To this end, we have used our statistical indicators along with 6000 simulated maps equipped with non-Gaussianity of local type with various amplitudes. From these simulated maps, which include the Gaussian one ($f_{\text{NL}}^{\text{local}} = 0$), we have generated 6000 S maps and 6000 K maps (see, e.g., Fig. 1), calculated the associated low ℓ mean power spectra S_ℓ and K_ℓ , made a study of the sensitivity and strength, and determined the limitations of non-Gaussian estimators S and K . By using the mean power spectra of the simulated non-Gaussian maps along with the χ^2 test of goodness, we

have shown that S and K indicators can be used to detect deviation from Gaussianity of local type for, typically, $f_{\text{NL}}^{\text{local}} \geq 500$ (see Fig. 3 and Table I). Thus, our indicators do not have enough sensitivity to detect deviation from Gaussianity of local type with the nonlinear parameter within the 7 yr WMAP bounds. This makes it apparent that the bispectrum based estimator employed by the WMAP team is more sensitive to primordial non-Gaussianity of local type than the S and K .

However, by using the same procedure, which is based upon the skewness S and kurtosis indicators K of patches of the CMB sky sphere, we have shown that these indicators do not have enough sensitivity to capture non-Gaussianity when the nonlinear parameter $f_{\text{NL}}^{\text{local}}$ lies within the 95% confidence level interval reported by the WMAP team [21] (cf. Fig. 4 and Table II). The positive outcome of the analysis performed in our previous works [13,14], together with the present outcome, seems to indicate that the deviation from Gaussianity captured in Refs. [13,14] is not of primordial nature, although it might have a primordial component.

Finally, we have also made a comparative study of non-Gaussianity of simulated maps and of the WMAP full-sky foreground-reduced 7 yr ILC map [16], which is summarized in Fig. 5 and Table III. An interesting outcome of this analysis is that the level of non-Gaussianity of ILC-7 yr ($f_{\text{NL}}^{\text{local}} \sim 775$) is higher than that of the simulated maps for $f_{\text{NL}}^{\text{local}}$ within observational bounds [21]. This renders quantitative information about the suitability of the foreground-reduced maps as Gaussian reconstruction of the full-sky CMB.

ACKNOWLEDGMENTS

M. J. R. acknowledges the support of FAPERJ under a CNE E-26/101.556/2010 grant. This work was also supported by Conselho Nacional de Desenvolvimento Científico e Tecnológico (CNPq)—Brazil, under Grant No. 475262/2010-7. A. B. thanks FAPEMIG for Grant No. APQ-01893-10. M. J. R. and A. B. thank CNPq for the grants under which this work was carried out. We are grateful to A. F. F. Teixeira for reading the manuscript and indicating some omissions and typos. Some of the results in this paper were derived using the HEALPIX package [33]. We also acknowledge the use of the Legacy Archive for Microwave Background Data Analysis.

APPENDIX

Here we present the results of a comparative analysis of deviation from Gaussianity performed by using Q, V, W band maps and simulated maps equipped with non-Gaussianity of local type for $f_{\text{NL}}^{\text{local}} = -10$ and 74, which are the WMAP-7 yr bounds for $f_{\text{NL}}^{\text{local}}$. As the calculations are similar to those of Sec. IV, we refer the readers to that section for more details on how they are made.

TABLE IV. Results of the reduced χ^2 test of the goodness of fit for the mean power spectra S_ℓ and K_ℓ as compared with the corresponding mean values obtained from MC simulated CMB input maps with $f_{\text{NL}}^{\text{local}} = 0$. Full-sky simulated maps were used.

Full-sky map	χ^2 for S_ℓ	χ^2 for K_ℓ
$f_{\text{NL}}^{\text{local}} = 500$	2.10	2.12×10
$f_{\text{NL}}^{\text{local}} = 1000$	3.02×10	5.50×10^2
$f_{\text{NL}}^{\text{local}} = 5000$	5.54×10^3	1.31×10^6

TABLE V. Results of the reduced χ^2 test of the goodness of fit for the mean power spectra S_ℓ and K_ℓ as compared with the corresponding mean values obtained from MC simulated CMB input maps with $f_{\text{NL}}^{\text{local}} = 0$. The simulated input maps were masked with the KQ75-7 yr mask.

Masked map	χ^2 for S_ℓ	χ^2 for K_ℓ
$f_{\text{NL}}^{\text{local}} = 500$	3.40×10	5.67×10^2
$f_{\text{NL}}^{\text{local}} = 1000$	4.69×10	6.81×10^2
$f_{\text{NL}}^{\text{local}} = 5000$	3.79×10^3	4.79×10^5

A word of clarification is in order before proceeding to the comparative analysis. In order to have an estimation of the role of the masking process in simulated maps with large values $f_{\text{NL}}^{\text{local}}$, we have calculated the reduced χ^2 of the mean S_ℓ and K_ℓ for maps endowed with $f_{\text{NL}}^{\text{local}} = 500, 1000, 5000$ without and with the KQ75-7 yr mask. These values quantify collectively the deviation from Gaussianity relative to MC Gaussian simulated maps ($f_{\text{NL}}^{\text{local}} = 0$). Tables IV and V contain the results of our calculations. These tables show that the greater $f_{\text{NL}}^{\text{local}}$ is, the smaller the ratio is between χ^2 values calculated for masked and unmasked simulated maps, respectively. Hence, the relative role of non-Gaussianity induced by the KQ75-7 yr mask in simulated maps is smaller for higher values of $f_{\text{NL}}^{\text{local}}$, as we expected from the outset. Thus, the role of the masking process should be bigger for $f_{\text{NL}}^{\text{local}}$, taking the lower and upper bound values of the WMAP-7 yr, an issue that will be discussed in the following.

We begin the above-mentioned comparative analysis by recalling that one either has the full-sky *contaminated* (Q, V, W) band maps to compare with full-sky simulated maps, or one masks both band and simulated maps. While in the former we have foreground maps that are quite contaminated, in the latter an induced non-Gaussianity arises from masking the simulated map process.

We have gathered together in Table VI the values of reduced χ^2 for the full-sky Q, V, and W frequency maps along with the values of the reduced χ^2 for maps endowed with non-Gaussianity for $f_{\text{NL}}^{\text{local}} = -10$ and 74. This table shows that the full-sky Q, V, and W band maps present a non-Gaussianity, as captured by our indicators, of several orders of magnitude higher than those of simulated maps for the lower and upper bound values of $f_{\text{NL}}^{\text{local}}$ obtained

TABLE VI. Results of the reduced χ^2 test of the goodness of fit for S_ℓ and K_ℓ calculated from Q, V, and W band maps and MC simulated maps for the lower and upper bound values of $f_{\text{NL}}^{\text{local}}$ obtained from WMAP-7 yr data. These values quantify collectively the deviation from Gaussianity relative to MC Gaussian simulated maps ($f_{\text{NL}}^{\text{local}} = 0$). Full-sky simulated and frequency maps were used.

Full-sky map	χ^2 for S_ℓ	χ^2 for K_ℓ
$f_{\text{NL}}^{\text{local}} = -10$	2.80×10^{-5}	4.80×10^{-5}
$f_{\text{NL}}^{\text{local}} = +74$	1.10×10^{-3}	1.00×10^{-2}
Q	8.79×10^{14}	1.75×10^{23}
V	6.15×10^{14}	3.17×10^{23}
W	3.14×10^{13}	9.14×10^{21}

from WMAP-7 yr data. Clearly, this is not a surprising result since the full-sky Q, V, and W band maps are very foreground contaminated, but it shows the suitability of our skewness and kurtosis indicators to detect such a huge difference in the levels of non-Gaussianity.

We have collected together in Table VII the results of the calculations of the reduced χ^2 for masked maps of the Q, V, and W bands, and for simulated input maps with $f_{\text{NL}}^{\text{local}} = -10$ and 74. Tables VI and VII show that, as expected, the KQ75-7 yr mask reduced significantly the levels of non-

TABLE VII. Results of the reduced χ^2 test of the goodness of fit for S_ℓ and K_ℓ calculated from Q, V, and W band maps and MC simulated maps for WMAP-7 yr lower and upper bound values of $f_{\text{NL}}^{\text{local}}$. The KQ75-7 yr mask was used for both frequency and simulated maps. These values quantify collectively the deviation from Gaussianity relative to MC Gaussian simulated maps ($f_{\text{NL}}^{\text{local}} = 0$).

Masked map	χ^2 for S_ℓ	χ^2 for K_ℓ
$f_{\text{NL}}^{\text{local}} = -10$	0.79	0.59
$f_{\text{NL}}^{\text{local}} = +74$	0.90	0.85
Q	4.04	3.20
V	0.86	0.56
W	0.73	0.60

Gaussianity of bands maps, bringing them down several orders of magnitude. Even with the mask, the detected level of non-Gaussianity for Q band maps is about 4 times the small level of the simulated masked maps for the WMAP-7 yr upper bound. As for the V and W bands and simulated maps, Table VII shows that these band maps present deviations from Gaussianity, as measured by our indicators, of similar order to those of maps with $f_{\text{NL}}^{\text{local}}$ in the WMAP-7 yr interval.

-
- [1] E. Komatsu, *Classical Quantum Gravity* **27**, 124010 (2010).
- [2] M. Liguori, E. Sefusatti, J.R. Fergusson, and E.P.S. Shellard, *Adv. Astron. Astrophys.* **2010**, 980523 (2010).
- [3] Xingang Chen, *Adv. Astron. Astrophys.* **2010**, 638979 (2010).
- [4] V. Desjacques and U. Seljak, *Classical Quantum Gravity* **27**, 124011 (2010).
- [5] P. Creminelli and M. Zaldarriaga, *J. Cosmol. Astropart. Phys.* **10** (2004) 006.
- [6] K. Koyama, S. Mizuno, F. Vernizzi, and D. Wands, *J. Cosmol. Astropart. Phys.* **11** (2007) 024; E.I. Buchbinder, J. Khoury, and B.A. Ovrut, *Phys. Rev. Lett.* **100**, 171302 (2008); J.-L. Lehners and P.J. Steinhardt, *Phys. Rev. D* **77**, 063533 (2008); J.-L. Lehners, *Phys. Rep.* **465**, 223 (2008); Y.-F. Cai, W. Xue, R. Brandenberger, and X. Zhang, *J. Cosmol. Astropart. Phys.* **05** (2009) 011.
- [7] C.L. Bennett *et al.*, *Astrophys. J. Suppl. Ser.* **148**, 97 (2003).
- [8] S.M. Leach *et al.*, *Astron. Astrophys.* **491**, 597 (2008).
- [9] E. Komatsu *et al.*, *Astrophys. J. Suppl. Ser.* **148**, 119 (2003).
- [10] M. Su, A.P.S. Yadav, M. Shimon, and B.G. Keating, *Phys. Rev. D* **83**, 103007 (2011).
- [11] PLANCK Collaboration, arXiv:astro-ph/0604069.
- [12] G.F.R. Ellis, *Gen. Relativ. Gravit.* **2**, 7 (1971); M. Lachièze-Rey and J.-P. Luminet, *Phys. Rep.* **254**, 135 (1995); G.D. Starkman, *Classical Quantum Gravity* **15**, 2529 (1998); J. Levin, *Phys. Rep.* **365**, 251 (2002); M.J. Rebouças and G.I. Gomero, *Braz. J. Phys.* **34**, 1358 (2004); M.J. Rebouças, *AIP Conf. Proc.* **782**, 188 (2005).
- [13] A. Bernui and M.J. Rebouças, *Phys. Rev. D* **79**, 063528 (2009).
- [14] A. Bernui and M.J. Rebouças, *Phys. Rev. D* **81**, 063533 (2010).
- [15] A. Bernui, B. Mota, M.J. Rebouças, and R. Tavakol, *Astron. Astrophys.* **464**, 479 (2007); *Int. J. Mod. Phys. D* **16**, 411 (2007).
- [16] B. Gold *et al.*, *Astrophys. J. Suppl. Ser.* **192**, 15 (2011).
- [17] J. Kim, P. Naselsky, and P.R. Christensen, *Phys. Rev. D* **77**, 103002 (2008).
- [18] J. Delabrouille *et al.*, *Astron. Astrophys.* **493**, 835 (2009).
- [19] G. Hinshaw *et al.*, *Astrophys. J. Suppl. Ser.* **180**, 225 (2009).
- [20] F. Elsner and B.D. Wandelt, *Astrophys. J. Suppl. Ser.* **184**, 264 (2009).
- [21] E. Komatsu *et al.*, *Astrophys. J. Suppl. Ser.* **192**, 18 (2011).
- [22] J.M. Bardeen, *Phys. Rev. D* **22**, 1882 (1980); J.M. Bardeen, J.R. Bond, N. Kaiser, and A.S. Szalay, *Astrophys. J.* **304**, 15 (1986).
- [23] H. Kodama and M. Sasaki, *Prog. Theor. Phys. Suppl.* **78**, 1 (1984).

- [24] R.K. Sachs and A.M. Wolfe, *Astrophys. J.* **147**, 73 (1967); see also Chap. 8 in [arXiv:hep-ph/0210162](#).
- [25] D.H. Lyth, C. Ungarelli, and D. Wands, *Phys. Rev. D* **67**, 23503 (2003).
- [26] M. Liguori, S. Matarrese, and L. Moscardini, *Astrophys. J.* **597**, 57 (2003).
- [27] M. Liguori, A. Yadav, F.K. Hansen, E. Komatsu, S. Matarrese, and B. Wandelt, *Phys. Rev. D* **76**, 105016 (2007); **77**, 029902(E) (2008).
- [28] E. Komatsu, D. N. Spergel, and B. D. Wandelt, *Astrophys. J.* **634**, 14 (2005); A. P. S. Yadav and B. D. Wandelt, *Phys. Rev. Lett.* **100**, 181301 (2008); A. P. S. Yadav, E. Komatsu, B. D. Wandelt, M. Liguori, F. K. Hansen, and S. Matarrese, *Astrophys. J.* **678**, 578 (2008); L. Senatore, K. M. Smith, and M. Zaldarriaga, *J. Cosmol. Astropart. Phys.* 01 (2010) 028.
- [29] E. Komatsu and D. N. Spergel, *Phys. Rev. D* **63**, 063002 (2001).
- [30] C.L. Bennett *et al.*, *Astrophys. J. Suppl. Ser.* **148**, 1 (2003).
- [31] G. Hinshaw *et al.*, *Astrophys. J. Suppl. Ser.* **170**, 288 (2007).
- [32] C. R ath, G. Rossmanith, G. Morfill, A. J. Banday, and K. M. G orski, [arXiv:1005.2481](#); C. R ath, G. E. Morfill, G. Rossmanith, A. J. Banday, and K. M. G orski, *Phys. Rev. Lett.* **102**, 131301 (2009); G. Rossmanith, C. R ath, A. J. Banday, and G. Morfill, *Mon. Not. R. Astron. Soc.* **399**, 1921 (2009); C. R ath, P. Schuecker, and A. J. Banday, *Mon. Not. R. Astron. Soc.* **380**, 466 (2007).
- [33] K. M. G orski, E. Hivon, A. J. Banday, B. D. Wandelt, F. K. Hansen, M. Reinecke, and M. Bartelman, *Astrophys. J.* **622**, 759 (2005).